Ferromagnetism in Bi_2Se_3:Mn epitaxial layers

H. J. von Bardeleben and J. L. Cantin
Institut des Nanosciences de Paris (INSP), Université Pierre et Marie Curie, 4, place Jussieu, 75005, Paris, France

D. M. Zhang,* A. Richardella, D. W. Rench, and N. Samarth
Department of Physics, Penn State University, University Park, Pennsylvania 16802, USA

J. A. Borchers
National Institute of Standards and Technology, Gaithersburg, Maryland 20899, USA
(Received 17 May 2013; revised manuscript received 6 August 2013; published 30 August 2013)

The magnetism in ~1 at% Mn-doped nanometric Bi_2Se_3 epitaxial layers has been studied by ferromagnetic resonance (FMR), magnetometry, and polarized neutron reflectivity (PNR) measurements. The FMR results reveal the formation of an intrinsic homogeneous FM bulk phase, as confirmed by the PNR measurements. Its critical temperature is low: $T_c \approx 6$ K; no surface magnetic phase is detected above this temperature. The FMR measurements at $T = 4.2$ K show a single uniform mode spectrum with a strong uniaxial in-plane/out-of-plane symmetry. The uniaxial anisotropy field at $T = 4$ K is $H_a \sim -2500$ Oe, corresponding to a uniaxial anisotropy constant of -9×10^3 erg/cm^3. The easy axis of magnetization is oriented in the film plane for temperatures between 4 K and T_c. Conduction electron-mediated FM in this (very) diluted magnetic semiconductor is considered as the most probable origin of the FM phase formation.

DOI: 10.1103/PhysRevB.88.075149 PACS number(s): 71.28.+d, 76.50.+g, 75.50.Dd

I. INTRODUCTION

The Bi-chalcogenides such as Bi_2Se_3 and Bi_2Te_3, long known for their thermoelectric properties, have recently gained much attention as canonical three-dimensional (3D) topological insulators (TIs) whose surfaces host Dirac electrons in spin-textured states.[1,2] These surface states can be modified by the breaking of time-reversal symmetry due to coupling with ferromagnetism (FM)[3] and can also themselves mediate long ranged FM order between magnetic dopants.[4–7] Experimental studies of such phenomena are still at a nascent stage.

Very recently it has been shown[8,9] that Mn doping allows obtaining FM phases in molecular beam epitaxy-grown Bi_2Se_3 films, but the magnetic properties were not yet fully understood and seemed contradictory. In particular, surface-sensitive measurements revealed magnetic properties quite different from those seen in bulk sensitive superconducting quantum interference device (SQUID) measurements. Further, the homogeneity of the Mn distribution has been questioned as secondary ion mass spectroscopy measurements had shown a surface accumulation of the Mn dopant in the first quintuple layer (QL). Thus, an in-depth study of the bulk properties seemed to be mandatory even for a more complete understanding of the surface-sensitive measurements. For this reason, we have undertaken combined SQUID, FM resonance (FMR), and polarized neutron reflectivity (PNR) measurements on samples similar to those used in Refs. 8 and 9, which have allowed us to clarify these issues. Our results show clearly that the surface-sensitive measurements of Ref. 8 were performed in a temperature region where the bulk of the layers was no longer FM. The surface magnetization of a standard 40-QL-thick Bi_2Se_3:Mn (1 at%) film is very weak with values in the 10^{-8} emu/cm^2, whereas the bulk has a magnetization close to 10^{-6} emu/cm^2 (see Ref. 9). Such small values are below the limit of detection for FMR and PNR measurements; indeed, no signals were observed by us above the critical temperature of the bulk phase, which was not higher than 6 K. The nature of the magnetic phase of the bulk part, which is the object of this study, was still an open question, and we show here that FMR provides much information on its origin.

We also address the question on the origin of the magnetic interactions. Whereas mean field calculations[6] had predicted a carrier mediated intrinsic FM ordering in 5 at% transition metal (TM) doped n-type Bi_2Se_3 and Bi_2Te_3, a clear experimental confirmation was still missing. It is *a priori* not evident that such an intrinsic FM phase can be achieved at all in a TI such as Bi_2Se_3 by doping with 3d TMs. A main experimental limitation might be a low solubility limit for 3d TM dopants in Bi_2Se_3, which would exclude achieving at% doping levels; however, even if this could be achieved by specific growth conditions, further complications might arise because of the existence of multiple lattice sites and associated charge and spin states. It is generally believed that 3d TM will substitute for Bi atoms and take the 3+ charge state. However, previous experience with diluted magnetic semiconductor materials has shown that more complicated situations with precipitates and secondary phase formation can easily occur at such high doping levels. In addition, Bi_2Se_3 is known to grow easily nonstoichiometric leading to high n-type conductivity attributed to Se-vacancy formation. The generally noncontrolled n-type carrier concentration can be expected to be an additional parameter influencing the FM properties. Thus, it is not astonishing that previous studies on heavily TM (Fe, Cr, Mn) doped TIs such as Bi_2Se_3 and Bi_2Te_3 had led to contradictory results: paramagnetic, spin glass, and FM secondary phases had all been evidenced.[9–14] The FM phase in Fe-doped Bi_2Se_3 bulk samples has been shown to be extrinsic and is being introduced by the formation of $Fe_{1-x}Se$ inclusions.[14]

In most previous studies, the magnetic phases were only studied by magnetometry (SQUID) measurements, and

techniques such as FMR have not yet been applied. The interest of FMR is its higher sensitivity and its resonant character, which allows distinguishing homogenous phases from FM precipitates. We have applied the FMR technique here to the study of at% Mn-doped Bi_2Se_3 epitaxial films of different thicknesses between 3 and 40 nm in order to investigate the magnetic phases and assess their characteristic parameters.

II. EXPERIMENTAL DETAILS

The Bi_2Se_3 films were grown by molecular beam epitaxy (MBE) on (111) oriented GaAs substrates on which a ZnSe buffer layer has first been deposited. The Bi/Mn beam equivalent pressure ratio was chosen to be ∼16, which corresponds to a targeted Mn concentration of ∼1 at% in the bulk. As the films were not Se capped, they were kept under vacuum to avoid oxidation. However, their properties did not change over a period of several months during which they were frequently transferred in air to the measuring cryostat. X-ray diffraction measurements confirmed that the rhombohedral layer structure ($R\bar{3}m$) of Bi_2Se_3 was preserved in the Mn-doped layers with lattice constants slightly modified by the Mn doping. The *c* axis of the layers is oriented perpendicular to the growth plane, and 180°-rotated twin domains can be observed by transmission electron microscopy. Secondary ion-mass spectroscopy and photoelectron emission spectroscopy analysis show that the films were homogeneously doped, with the exception of a surface layer (⩽1 nm), in which an accumulation of Mn atoms occurred. Films of 3, 8, 15, and 40 nm have been studied. The films are *n*-type conductive with carrier concentrations in the 10^{19} to 10^{20} cm^{-3} range. More details on the film growth and characterization have been previously reported.[9,15]

The FMR measurements have been performed with an X-band (9 GHz) spectrometer applying standard field modulation techniques. The lowest temperature obtainable with our set-up was 4.2 K. The FMR measurements were performed in the temperature range 4.2 K to 40 K on samples of typically 2 × 5-mm^2 dimension. We measured the angular variations of the FMR spectra for the two rotation planes ($1\bar{1}00$) and (0001). Magnetization measurements by SQUID have been performed in the temperature range 1.8 K to 20 K.

III. MAGNETOMETRY AND FMR RESULTS

First, we recall the results of the SQUID measurements; results obtained on very similar samples have been published recently.[9] Both hysteresis cycles and temperature-dependent $M(T)$ measurements have been performed (Fig. 1). To allow a direct comparison with the FMR measurements, the magnetization has been measured under an applied field of 6 kOe [Fig. 1(a)]; the application of the magnetic field will shift the ordering temperature to higher values. When measured at small fields (50 Oe), the critical temperature is found to be 5.8 K. The easy axis of magnetization is in-plane. The values of the saturation magnetization are small and do not exceed 4×10^{-7} emu/mm^2 at $T = 4.2$ K for the 40-nm film [Fig. 1(b)]; converting this result into volume concentrations—assuming a homogeneous distribution of the magnetization over the total layer thickness—we obtain values of ≈10 emu/cm^3 [Fig. 1(c)]. The previous secondary ion

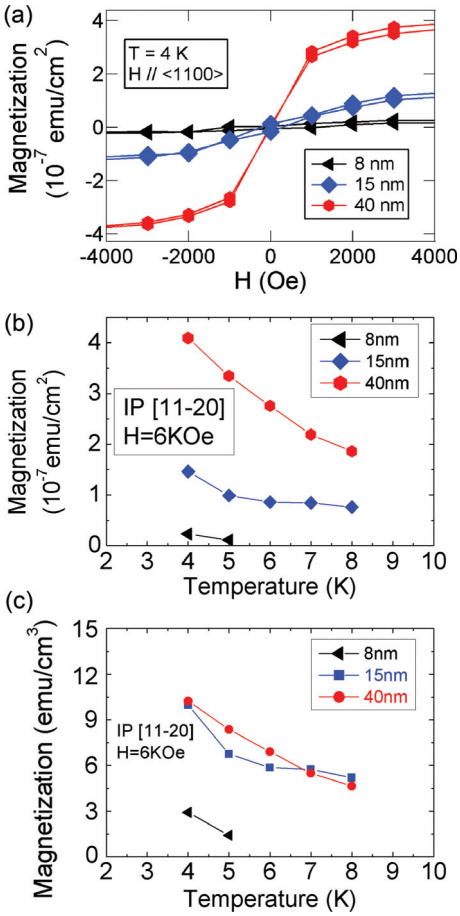

FIG. 1. (Color online) (a) Magnetization measurements of the 40-nm, 15-nm, and 8-nm Bi_2Se_3:Mn films at $T = 4$ K and H//[1100]; (b) temperature dependence of the magnetization (emu/cm^2) of the 40-nm film measured at an applied field of 6 kOe; (c) magnetization values in emu/cm^3 obtained by dividing by the layer thickness.

mass spectroscopy (SIMS) measurements[9] had shown a surface accumulation of the Mn doping in the first QL and homogeneous Mn concentration in the bulk of the layer. Thus, the actual magnetization of the bulk part might even be lower. As the magnetization of the Mn-enriched surface layer, which has a critical temperature much higher than the T_c bulk value of 5.8 K, is not detectable by the SQUID measurements above 6 K, its numerical value must, however, be negligible as compared to the bulk part. This validates our approach to deduce volume magnetization values (emu/cm^3) from the SQUID measurements. A value of 10 emu/cm^3 is very small as compared to 3d TM FM layers but is not unexpected for diluted magnetic semiconductors with a ∼1 at% doping level. At $T = 4.2$ K, the lowest temperature of the FMR measurements, the 40-nm and 15-nm films have the same magnetization of 10 emu/cm^3, whereas for the thinner 8-nm film this value decreased by a factor of 30. For the 3-nm sample, the magnetization is below the detection limit. This decrease for the thinnest layers is probably due to the fact that their critical temperature is below 1.8 K, the lowest temperature of the SQUID measurements.

In Fig. 2(a), we show typical FMR spectra observed at $T = 4.2$ K for the 40-nm-thick film. For all orientations of the

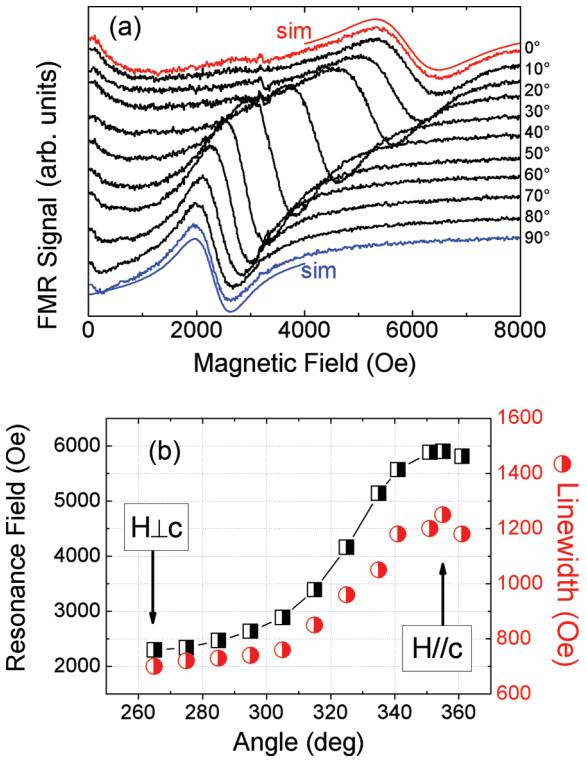

FIG. 2. (Color online) (a) FMR spectra of the 40-nm film measured at $T = 4.2$ K for a variation of the magnetic field in the (1100) plane and simulation by a Lorentzian for the two field orientations $H//c$ (red) and $H//$(see Refs. 10–19) (blue); (b) angular variation of the resonance fields and linewidth.

applied magnetic field, we observe one single, highly anisotropic Lorentzian line. Its resonance-field position [Fig. 2(b)] varies monotonously with the direction of the applied field. For $H//c$ (perpendicular to the film plane), the resonance field is close to 6000 Oe and decreases for $H\perp c$ to about 2300 Oe. The linewidth varies equally monotonously between 650 Oe ($H//c$) and 1200 Oe ($H\perp c$). This is the fingerprint of a uniform mode spectrum resulting from a homogeneously magnetized FM layer. The angular variation of the resonance fields shows that the hard axis of magnetization is perpendicular to the film plane, and the easy axis in the film plane which is in agreement with the SQUID results. From the FMR characteristics, we attribute this phase to the bulk part of the epitaxial layer

In Fig. 2, a fit with a Lorentzian of the experimental FMR spectra is shown for the two extreme orientations $H//[0001]$ and $H//[1\bar{1}00]$. For a rotation of the magnetic field in the (0001) growth plane, we observe a quasi-isotropic FMR spectrum. A more detailed analysis reveals a clear small sixfold symmetry (Fig. 3). The in-plane anisotropy field is only 40 Oe. This sixfold symmetry is well in line with the rhombohedral structure of the Bi_2Se_3 lattice given the two twin orientations present.

We have equally investigated the thickness dependence of the magnetic properties. In addition to the 40-nm film, we have measured the 15-nm, 8-m, and 3-nm films at $T \geqslant 4.2$ K. As expected from the magnetization data, only the 15-nm layer displays measurable FMR spectra [Fig. 4(a)]. The resonance fields and linewidth are very similar to those measured for

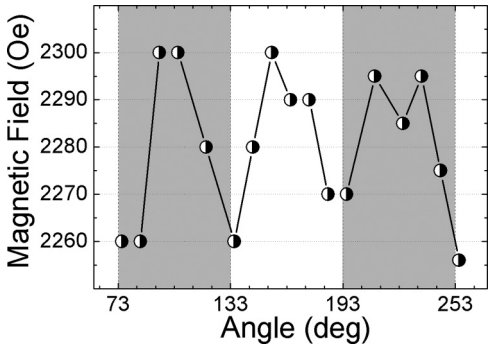

FIG. 3. Resonance fields of the 40-nm film for a variation of the magnetic field in the film plane as a function of the polar angle.

the 40-nm film [Fig. 4(b)]; however, the intensity of the FMR spectrum is divided by three, which is in good agreement with the approximately three times smaller thickness of this sample. As FMR is a quantitative technique and the intensity of the spectra obtained by a double integration of the first derivative FMR spectra is proportional to the total magnetic moment of a sample, this demonstrates equal magnetizations in these two samples. For the 8-nm and 3-nm samples, no FMR spectra are observed at $T = 4.2$ K, as expected from their very low magnetization values at this temperature.

To interpret the angular variation of the FMR spectra, we use the model of Chappert *et al.*[16] developed for the case of hcp Co films. It is based on the Smit Beljers formalism,[17]

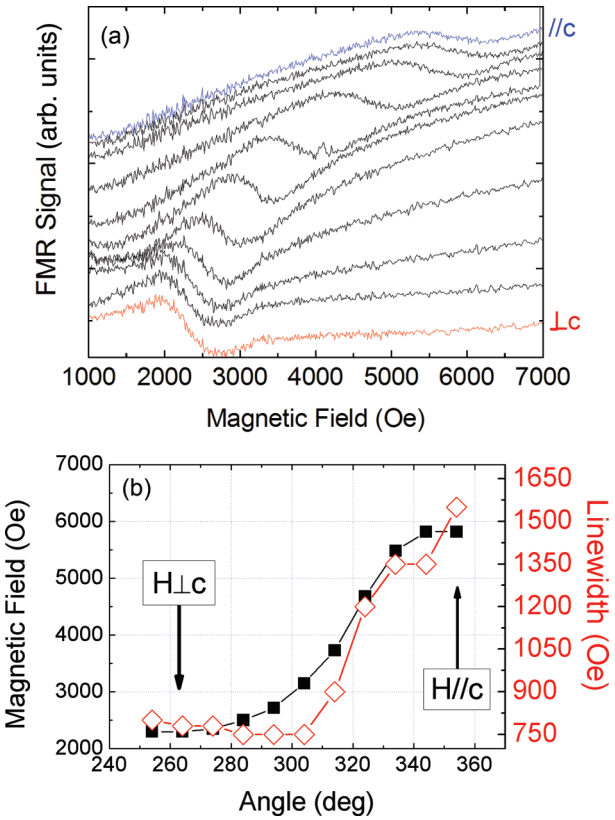

FIG. 4. (Color online) (a) FMR spectra of the 15-nm film at $T = 4.2$ K for a variation of the magnetic field from $H//c$ to $H\perp c$; (b) angular variation of the resonance fields and line width.

which derives the resonance positions from the energy density function $E(\varphi, \theta)$:

$$E = -HM\sin\theta\cos(\varphi_H - \varphi) + \tfrac{1}{2}4\pi M^2\sin^2\theta\sin^2\varphi - (K_1 + 2K_2)\sin^2\theta\sin^2\varphi + K_2\sin^4\theta\sin^4\varphi, \quad (1)$$

where K_1 and K_2 are the first- and second-order effective anisotropy constants, which include the contributions from the magnetocrystalline and strain-induced anisotropy; φ_H and θ_H are the polar and azimuthal angles of the applied magnetic field (H); and φ and θ are the angles of the magnetization vector M, respectively.

The equilibrium position of the magnetization is given by the relation

$$MH\sin(\varphi_H - \varphi_{eq}) = (4\pi M^2 - 2K_1 - 4K_2)\sin\varphi_{eq}\cos\varphi_{eq} + 4K_2\sin^3\varphi_{eq}\cos\varphi_{eq}, \quad (2)$$

and the resonance position is obtained from the relation

$$\left(\frac{\omega}{\gamma}\right)^2 = \frac{1}{M^2\sin^2\theta}\left\{\frac{\partial^2 E}{\partial\theta^2}\frac{\partial^2 E}{\partial\varphi^2} - \left[\frac{\partial^2 E}{\partial\theta\partial\varphi}\right]^2\right\}. \quad (3)$$

The angular variation of the uniform mode FMR spectra can be well fitted by this expression [Fig. 5(a)] and allows the determination of the anisotropy constants K_1 and K_2. At $T = 4$ K, we obtain for the 40-nm sample for K_1 a value of -8629 erg/cm^3 and for K_2 a value of -353 erg/cm^3. The negative sign of K_1 indicates that the c axis is the hard axis of magnetization and the easy axis is lying in the film plane. The corresponding anisotropy fields are -2576 Oe and -210 Oe, respectively. Due to the small value of the magnetization, the demagnetization field of $4\pi M = 126$ Oe related to the thin

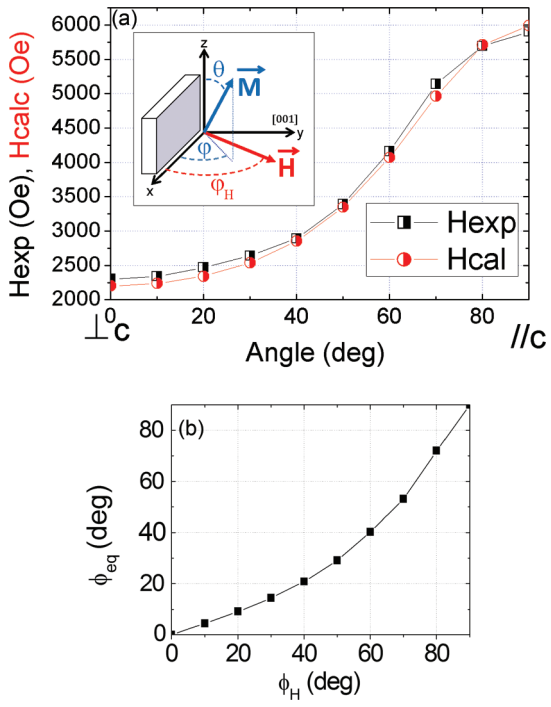

FIG. 5. (Color online) (a) 40-nm film at $T = 4.2$ K experimental resonance fields (black dots) and simulation (red dots) with Eq. (3); (b) equilibrium angle of the magnetization as a function of angle of the applied magnetic field.

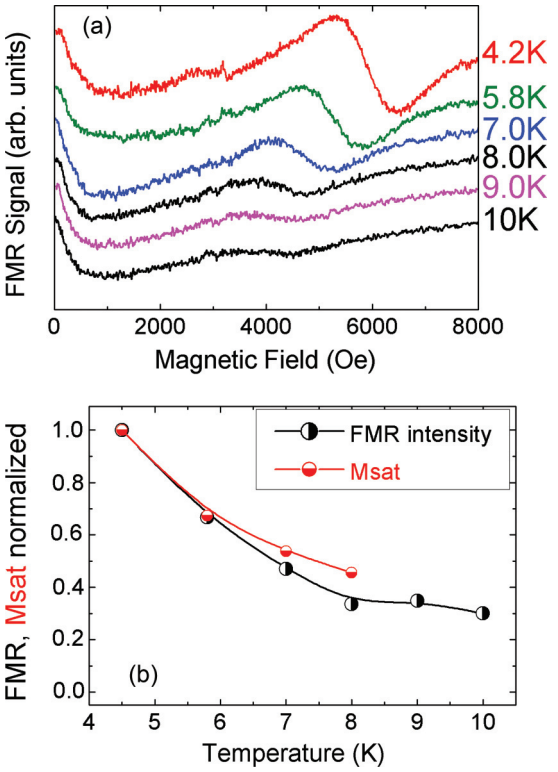

FIG. 6. (Color online) (a) Temperature dependence of the FMR spectra of the 40-nm film for $H//c$; (b) FMR intensity (black dots) and saturation magnetization M_{sat} (red dots) normalized at $T = 4.2$ K as a function of temperature.

film geometry is not dominant for the easy axis orientation. The distinction between the intrinsic and strain-induced parts of the uniaxial anisotropy field in the Bi_2Se_3 layer requires further investigations. As shown in Fig. 5(b), the magnetization is only aligned with the applied magnetic field for the two orientations in-plane and out-of plane.

The angular variation of the FMR linewidth demonstrates a strong influence of inhomogeneous broadening, which leads to highly increased linewidth for $H//c$ as compared to $H\perp c$. Such a behavior has often been observed in other DMS systems[18–20] and can be attributed to the local variation of the internal magnetic fields[21] related to the random incorporation of the Mn dopant over the Bi lattice sites.

The temperature dependence of the FMR spectra has equally been investigated. In Fig. 6(a), we show the uniform mode spectra of the 40-nm sample between 4.2 K and 10 K. We observe a shift of the resonance positions toward the paramagnetic limit and a decrease in the line intensity. The FMR intensity obtained by a double integration of the experimental spectra is proportional to the magnetization and can thus be compared to the SQUID results. In Fig. 6(b), we compare the evolution of these quantities normalized to their value at $T = 4.2$ K. It can be seen that both follow the same temperature dependence, which confirms that both are related and belong to the FM bulk phase.

As previously published, x-ray magnetic circular dichroism (XMCD) measurements performed[8] on similar samples had indicated a surface FM with much higher critical temperatures reaching 40 K; we have equally investigated these samples

in this temperature range. However, in agreement with the SQUID results, which did not show measurable magnetization for $T > 6$ K, we did not observe any additional FMR spectrum above the T_c of the bulk part.

IV. PNR RESULTS

The nature of the FM was further studied by PNR at the NIST Center for Neutron Research. The net in-plane magnetization of the 15-nm-thick sample was studied at 5 K and 20 K in a 0.8 T in-plane field with a neutron wavelength $\lambda = 4.75$ Å.

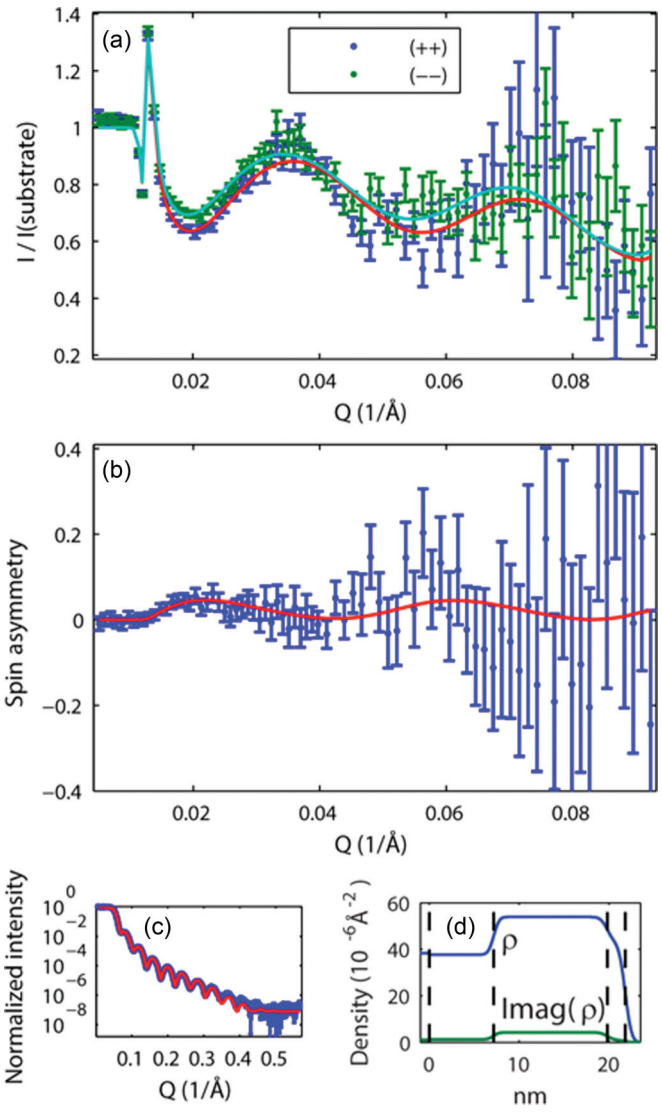

FIG. 7. (Color online) (a) Neutron reflectivity of the 15-nm-thick sample at 5 K plotted on a normalized Fresnel scale (reflected intensity divided by the reflectivity of the substrate) to help bring out the features at higher Q. (b) Spin asymmetry between the spin-up (++) and spin-down channels (− −). The splitting near 0.02 (1/Å) can only be explained by magnetism in the bulk of the sample. (c) X-ray reflectivity fit used to determine the thicknesses of the layers in the sample. The best fit is achieved with a lower density in the last few nm of the Mn-doped Bi_2Se_3. (d) Sample density inferred from XRR. Vertical dashed lines indicate the interfaces between GaAs (0 nm), ZnSe, Bi2Se3, and a near-surface Bi_2Se_3 layer.

Incident neutrons were polarized parallel (+) or antiparallel (−) to the applied field, and polarized scattered intensities were measured. The reflectivity curves were then fit to a model that included the structure of the sample [verified by x-ray reflectivity (XRR) measurements] and its magnetization. The net magnetization was deduced from asymmetry between nonspin flip channels (+ +) and (− −), while the negligible signal in the spin flip (+ −) and (− +) channels indicated that the moment was aligned in-plane along the external field direction.

Due to the similar neutron scattering length densities (SLD) of the component layers, the neutron reflectivity does not show much structural contrast as compared to XRR. The combined structural and magnetic features are best seen, therefore, by plotting the data on a Fresnel scale [Fig 7(a)]. The splitting seen between the (+ +) and (− −) channels at low Q ($Q \equiv 4\pi \sin(\theta)/\lambda$, where θ is the angle of reflection) at 5 K can only be explained by the bulk of the material being magnetic, which is consistent with the FMR results. The bulk magnetic SLD is found to be 2.5×10^{-8} Å^{-2}, corresponding to a magnetization of 8.6 emu/cm^3, consistent with both FMR and SQUID. No measureable splitting was observed at 20 K.

The XRR data is best fit with a decrease in the Bi_2Se_3 layer density in the sample surface region [Figs. 7(c) and 7(d)], consistent with the SIMS measurements, which showed an increased Mn density near the surface. The PNR suggests some signs of FM in this near surface region, but these are dependent on the details of the model and are currently being further investigated.

V. DISCUSSION

Our FMR results show that Mn doping in the 1 at% range of MBE grown n^+-type epitaxial Bi_2Se_3 layers can induce a long-range ordered FM state. These layers have all the characteristics of a diluted FM semiconductor such as the prototype material GaMnAs. FMR spectroscopy has been applied in the past successfully for diluted semiconductors such as GaAs:Mn (Refs. 18 and 19) and GaAsP:Mn.[20] These materials have been shown to become intrinsic FM semiconductors above a threshold-doping level of typically 2 at% Mn. They possess a much lower solubility limit, and in order to introduce such a high (>2 at%) Mn concentration, nonequilibrium growth techniques such as low temperature MBE are required to avoid Mn precipitation and secondary phase formation.[21] Such an approach has not yet been attempted for TIs but might be of interest at least for the case of Fe doping. The mechanism for the FM phase formation has been established because of a carrier-induced exchange interaction between the high spin Mn^{2+} ions.[22] The particularity of these two compounds is that the Mn dopants, when substituting for Ga atoms, introduce magnetic ions ($Mn^{2+}/S = 5/2$) and free carriers (holes) of comparable concentration at the same time. If the hole concentration is selectively decreased, which can be achieved by hydrogen annealing, the films become paramagnetic for carrier concentration below typically $<10^{19}$cm^{-3} (see Ref. 19). In the case of Bi_2Se_3:Mn, the electrical activity and its potential site dependence of the Mn dopant has not yet been determined. The observed high n-type carrier concentration is assumed to be related to nonstoichiometry effects, but the related defect Se vacancy, Se antisite, or interstitials have not yet been identified.

As we are in a diluted doping range, a direct exchange interaction between close nearest-neighbor Mn atoms seems improbable. It seems clear, however, that a carrier-mediated exchange interaction in these highly *n*-type conductive layers are at its origin. As the carrier concentration is due to the donor action of nonstoichiometry-related intrinsic defects, growth conditions are crucial for establishing a FM phase. Further, as Bi site-substituted Mn ions are expected to act as acceptors, Mn doping levels in excess of the native donor concentration might lead to the suppression of the FM phase due to electrical compensation. In *n*-type material, such as our case, Mn_{Bi} ions will be negatively charged, i.e., Mn^{2+}, with a high spin $S = 5/2$ groundstate.

In a previous publication[9] on very similar samples, the FM phase observed by SQUID measurements had been attributed to a narrow near-surface region. In the light of the additional results presented here, this has to be revised, and the FM is clearly associated with the bulk of the layer, which is quite homogeneously doped. The high temperature ($T \geqslant 40$ K) FM phase evidenced by XMCD measurements,[8] characterized by a critical temperature higher than 100 K and a different easy-axis orientation of the magnetization, out-of-plane as compared to the in-plane orientation for the bulk of the layer, must be of a different origin. As the SIMS measurements had shown a nearly one order of magnitude higher Mn-surface concentration, it cannot be excluded that a different phase might have been formed at the surface. Further surface-specific structure measurements are required to investigate this issue.

VI. CONCLUSION

In conclusion, FMR spectroscopy has shown, in agreement with PNR measurements, that a homogeneous intrinsic FM phase can be introduced in epitaxial *n*-type Bi_2Se_3 MBE grown layers by at% Mn doping. The easy axis of magnetization is oriented in the film plane due to a strong build-in uniaxial anisotropy. The effect of demagnetization fields is negligible for the easy-axis orientation. The origin of the FM interaction is attributed to a carrier-mediated exchange interaction similar to the case of GaMnAs. Bi_2Se_3 would be a rare case of a FM DMS with conduction electron-induced coupling.

ACKNOWLEDGMENTS

This work was supported by DARPA (N66001-11-1-4110). We also acknowledge partial support from ONR (N00014-12-1-0117) and the Penn State Center for Nanoscale Science under the MRSEC program (NSF Grant No. DMR-0820404). This publication was also supported by the Pennsylvania State University Materials Research Institute Nanofabrication Laboratory and the National Science Foundation Cooperative Agreement No. ECS-0335765.

*Current address: Center for Nanoscale Science and Technology, National Institute of Standards and Technology, Gaithersburg, MD 20899, USA.

[1] M. Z. Hasan and C. L. Kane, Rev. Mod. Phys. **82**, 3045 (2010).
[2] X.-L. Qi and S.-C. Zhang, Rev. Mod. Phys. **83**, 1057 (2011).
[3] Q. Liu, C.-X. Liu, C. Xu, X.-L. Qi, and S.-C. Zhang, Phys. Rev. Lett. **102**, 156603 (2009).
[4] C. Niu, Y. Dai, M. Guo, W. Wei, Y. Ma, and B. Huang, Appl. Phys. Lett. **98**, 252502 (2011).
[5] G. Rosenberg and M. Franz, Phys. Rev. B **85**, 195119 (2012).
[6] M. Lasia and L. Brey, Phys. Rev. B **86**, 045317 (2012).
[7] J.-M. Zhang, W. Zhu, Y. Zhang, D. Xiao, and Y. Yao, Phys. Rev. Lett. **109**, 266405 (2012).
[8] S.-Y. Xu, M. Neupane, C. Liu, D. Zhang, A. Richardella, L. A. Wray, N. Alidoust, M. Leandersson, T. Balasubramanian, J. Sánchez-Barriga, O. Rader, G. Landolt, B. Slomski, J. H. Dil, J. Osterwalder, T.-R. Chang, H.-T. Jeng, H. Lin, A. Bansil, N. Samarth, and M. Z. Hasan, Nature Physics **8**, 616 (2012).
[9] D. Zhang, A. Richardella, D. W. Rench, S. Y. Xu, A. Kandala, T. C. Flanagan, H. Beidenkopf, A. L. Yeats, B. B. Buckley, P. V. Klimov, D. D. Awschalom, A. Yazdani, P. Schiffer, M. Z. Hasan, and N. Samarth, Phys. Rev. B **86**, 205127 (2012).
[10] J. Choi, H. W. Lee, B. S. Kim, S. Choi, J. Choi, J. H. Song, and S. Cho, J. Appl. Phys. **97**, 10D324 (2005).
[11] Y. S. Hor, P. Roushan, H. Beidenkopf, J. Seo, D. Qu, J. G. Checkelsky, L. A. Wray, D. Hsieh, Y. Xia, S. Y. Xu, D. Qian, M. Z. Hasan, N. P. Ong, A. Yazdani, and R. J. Cava, Phys. Rev. B **81**, 195203 (2010).
[12] P. Janicek, C. Drasar, P. Lostak, J. Vejpravova, and Y. Sechovsky, Physica B **403**, 3553 (2008).
[13] Z. Salman, E. Pomjakushina, V. Pomjakushin, A. Kanigel, K. Chashka, K. Conder, E. Morrenzoni, T. Proschka, K. Sedlak, and A. Suter, arXiv:1203.4850.
[14] H. Ji, J. M. Allred, N. Ni, J. Tao, M. Neupane, A. Wray, S. Xu, M. Z. Hasan, and R. J. Cava, Phys. Rev. B **85**, 165313 (2012).
[15] A. Richardella, D. M. Zhang, J. S. Lee, A. Koser, D. W. Rench, A. L. Yeals, B. B. Buckley, D. D. Awschalom, and N. Samarth, Appl. Phys. Lett. **97**, 262104 (2010).
[16] C. Chappert, K. L. Dang, P. Beauvillain, H. Hurdequint, and D. Renard, Phys. Rev. B **34**, 3192 (1986).
[17] J. Smit and H. G. Beljers, Philips Res. Rep. **10**, 115 (1955).
[18] X. Liu, Y. Y. Zhou, and J. K. Furdyna, Phys. Rev. B **75**, 195220 (2007).
[19] Kh. Khazen, H. J. von Bardeleben, J. L. Cantin, L. Thevenard, L. Largeau, O. Mauguin, and A. Lemaitre, Phys. Rev. B **77**, 165204 (2008).
[20] M. Cubukcu, H. J. von Bardeleben, Kh. Khazen, J. L. Cantin, O. Mauguin, L. Largeau, and A. Lemaitre, Phys. Rev. B **81**, 041202(R) (2010).
[21] S. Ye, P. J. Klar, Th. Hartmann, W. Heimbrodt, M. Lampalzer, S. Nau, T. Torunski, W. Stolz, T. Kurz, H. A. Krug von Nidda, and A. Loidl, Appl. Phys. Lett. **83**, 3927 (2003).
[22] T. Jungwirth, J. Sinova, J. Masek, J. Kucera, and A. H. MacDonald, Rev. Mod. Phys. **78**, 809 (2006).